*High Power Laser Science and Engineering*, (2024), Vol. 12, e64, 8 pages.
doi:10.1017/hpl.2024.54

HIGH POWER LASER SCIENCE AND ENGINEERING

**RESEARCH ARTICLE**

# Drift-free, 11 fs pulse delay stability in dual-arm PW-class laser systems

Andrei B. Nazîru[1,2], Ştefan Popa[1,2], Ana-Maria Lupu[1,2], Dan Gh. Matei[1], Alice Dumitru[1,2], Dmitrii Nistor[1,3], Antonia Toma[1], Lidia Văsescu[1], Ioan Dăncuş[1], Claudiu A. Stan[4], and Daniel Ursescu[1,2]

[1] *Extreme Light Infrastructure - Nuclear Physics, National Institute for Physics and Nuclear Engineering - Horia Hulubei, Măgurele 077125, Romania*

[2] *Doctoral School of Physics, University of Bucharest, Măgurele 077125, Romania*

[3] *Engineering and Applications of Lasers and Accelerators Doctoral School, National University of Sciences and Technology Politehnica Bucharest, Bucharest 060042, Romania*

[4] *Department of Physics, Rutgers University-Newark, Newark, New Jersey 07102, USA*

*(Received 18 October 2023; revised 1 August 2024; accepted 8 August 2024)*

**Abstract**

Simultaneous ultra-intense pulses at petawatt laser facilities enable a broad range of experiments in nuclear photonics and strong field quantum electrodynamics. These experiments often require very precise control of the time delays between pulses. We report measurements of the time delay between the two 1 PW outputs of the Extreme Light Infrastructure - Nuclear Physics (ELI-NP) facility in Romania. The short-term standard deviation of the time delay was approximately half of the pulse duration of 23 fs, and the average delay drifted with up to 100 fs/h. The drift and sporadic delay jumps were corrected using a feedback loop, which reduced the long-term standard deviation of the delay close to its short-term value. These results imply that in ELI-NP experiments using two simultaneous pulses, a temporal overlap of better than half of the pulse duration can be achieved for more than two thirds of the shots, which would enable high data rate experiments using simultaneous petawatt pulses.

**Keywords:** feedback control; high-power laser; laser synchronization; ultrashort laser pulses

## 1. Introduction

The highest laser pulse intensities demonstrated experimentally are above $10^{23}$ W/cm$^2$[1], and allow the generation of very strong electromagnetic fields that enable new experiments in strong field quantum electrodynamics[2–4]. Many of the proposed experiments also require multiple ultra-intense pulses, for example Compton scattering on laser accelerated electrons to observe radiation reactions or for other applications in nuclear photonics[5,6], multi-stage electron acceleration[7,8], multiple-pulse field enhancement[9] with subsequently enhanced proton acceleration[10], quantum vacuum studies[11] and photon–photon scattering[12]. Such experiments seem feasible using laser pulses with peak power in the petawatt (PW) range.

Several PW-class laser facilities include multiple amplification arms that can deliver two pulses simultaneously: Astra-Gemini[13], CoReLS[14,15], Arcturus[16], VEGA[17], HIGGINS[18] and Extreme Light Infrastructure - Nuclear Physics (ELI-NP)[19,20] in Romania. More facilities are being built or planned, including ZEUS[21], XCELS, SEL and SG-II SuperX[22]. Among them, the ELI-NP facility is a promising option for strong field experiments because of its high peak power. The high-power laser system (HPLS) at the ELI-NP facility features two amplification arms with independent compressors, which can be synchronized for dual output at 100 TW, 1 PW and 10 PW peak power.

The generation of the very strong electromagnetic fields required for experiments is realized by focusing the intense laser pulses available from these PW-class laser facilities. This limits the spatial extension of the field to a few micrometers, and the temporal extension to the laser pulse duration, which is typically a few tens of femtoseconds at PW-class facilities. For experiments with multiple pulses, it is critical to overlap the pulses temporally, or at least to measure the

Correspondence to: D. Ursescu, Extreme Light Infrastructure - Nuclear Physics, National Institute for Physics and Nuclear Engineering - Horia Hulubei, 30 Reactorului str., Măgurele 077125, Ilfov, Romania. Email: daniel.ursescu@eli-np.ro

delay between pulses for each shot and select for analysis only the shots with overlapping pulses.

Several techniques for precise delay measurements exist for high repetition rate fiber-based lasers, such as heterodyne detection[23], balanced optical cross-correlators[24,25] and spectral interference[26]. For example, Prakash *et al.*[24] measured a time delay jitter of 39 fs with a precision of 1.8 fs, using the spectral interference between two ultrashort pulses after 10 km propagation in optical fibers.

In high peak power laser systems, two classes of techniques have been used for delay measurements. The first class uses optical interference in the spatial or spectral domain. Short delays, while pulses overlap, can be measured from the visibility of the fringes, while longer delays can be measured via a Fourier analysis of the spectrum of the combined pulses[27]. This technique was used at the CoReLS facility to determine a jitter of 11 fs between compressed but not amplified pulses that traveled independently over a path of less than 24 m, and had a precision of 6 fs at 0–30 fs delay and 7 fs at 20–200 fs delay. A variation of this technique, based on spatio-spectral interference of the two focused pulses[28], was used at the Astra-Gemini facility and achieved an initial precision of $\pm 15$ fs[26]. This measurement was improved to measure a shot-to-shot jitter of $10.3 \pm 0.7$ fs between the two arms, with an initial resolution of 37 fs being reduced to less than 5 fs via zero-padding in the Fourier transform[29]. For the Arcturus laser system, a synchronization uncertainty of 300 fs was reported using optical interferometry and/or shadowgraphy. The second class encompasses approaches that do not rely solely on linear optics. At the HIGGINS facility, plasma waves generated in a gas with one pulse were imaged optically with the second pulse, which enabled the determination of the delay to a few hundred femtoseconds, and then a more precise measurement was made by imaging the plasma wave with an electron beam produced by the second pulse, from which a synchronization jitter of 13 fs between the two pulses was measured[30].

Here, we report a method to characterize the relative time delay between the pulses from a dual-arm ultrafast laser system. The method is based on a principle first reported by Ungureanu *et al.*[31], which combines spectral-temporal encoding with an ultrafast optical switch based on a plasma mirror induced on a transparent target. This method is related to a technique used at X-ray laser facilities to measure the time delay between X-ray and optical pulses, with better than 10 fs accuracy, by combining X-ray-induced photorefractive effects with optical-spectral or spatial encoding[32]. A similar method, known as FROST, uses transient absorption in solids to characterize the laser pulse duration[33]. Our experimental setup is compact (1 m in length) and can be installed at end-stations for online characterization.

We measured the relative time delay between the two pulses from 1 PW outputs at the ELI-NP facility after the pulse compressors, where the laser pulses propagated independently for 170 m each. This measurement is a good indicator of the pulse delay stability (DS) in user experiments, where the pulses will propagate 35–40 m further downstream from our measurement point, guided with only two large mirrors in vacuum. The short-term standard deviation of the delay was approximately half the pulse length. We also achieved long-term stability of the delay by using a feedback loop to correct drifts and jumps.

## 2. Methods

### 2.1. Laser system

The dual-arm 10 PW HPLS of the ELI-NP facility in Romania has an optical parametric chirped pulse amplification (OPCPA) front-end followed by six laser amplification stages and optical compressors. The HPLS can be configured for outputs of 100 TW, 1 PW or 10 PW, at repetition rates of 10 Hz, 1 Hz and 1/minute, respectively[19]. It is housed in a large room, 70 m long and 40 m wide, with controlled humidity and temperature stabilized within 0.5 K. The laser system is placed on two 40 m long passive-damping optical tables (Newport), which, in turn, are placed on an antivibration concrete floor of 0.6 m thickness, designed to suppress the vibrations by a factor of 100 from 1 to 200 Hz[34]. The laser system is encapsulated in boxes to reduce air turbulence.

Here we used the 1 PW outputs on both arms, and the schematic of this HPLS configuration is shown in Figure 1. The pulses were generated by the laser oscillator of the front-end B of the HPLS, amplified to 10 mJ, and then split into two 5 mJ pulses. The separated pulses then propagated through the first and second amplification stages on each arm, which are laid out in a mirrored configuration, and were guided to the delay measurement setup.

Since the delay measurements were performed in air, the pulses are not allowed to be at the 1 PW power level before being sampled for delay measurements, but we configured the HPLS to replicate closely the pulse propagation at high intensity. On both arms, all pump lasers used for 1 PW output (amplifiers A1.1, A1.2, A2) were active to replicate the thermal effects in the amplification crystals, except for one disabled pump laser (out of the six) in Arm B, amplifier A.2. The pulses propagating in Arm B were amplified in A1.1, A1.2 and A.2 to approximately 12 J. Pulses propagating in Arm A were amplified in A1.1 and A1.2 to approximately 1.5 J, and then further amplification was suppressed by desynchronizing the femtosecond pulse and the pulses from the pump lasers in A.2. Both pulses were then attenuated, using wedges, before reaching the optical compressor.

https://doi.org/10.1017/hpl.2024.54 Published online by Cambridge University Press

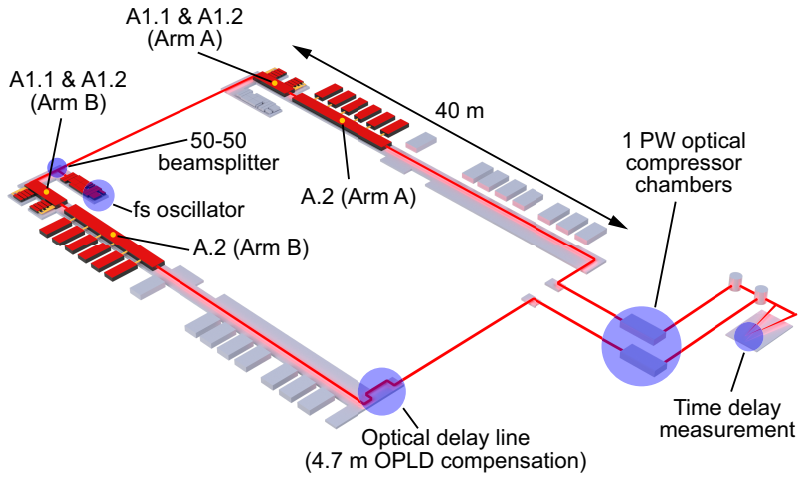


**Figure 1.** Configuration of the ELI-NP high-power laser system for 1 PW delay measurements. Two pulses split from the same seed pulse passed through the active amplifiers highlighted in red (A1.1 and A1.2, and A2), which are the ones used to produce the 1 PW output. An optical delay line provided a coarse compensation of the path length difference between the two arms. The measurements were performed after the output of the 1 PW optical compressors.

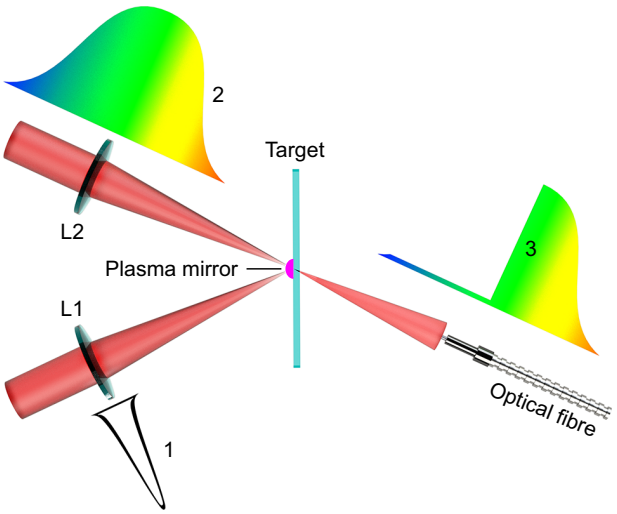


**Figure 2.** Principle of the temporal delay measurement. A temporally compressed pulse (1) and a temporally stretched chirped pulse (2) are focused by lenses (L1 and L2) on a transparent target. The short pulse generates a plasma mirror on the target, which reflects part of the chirped pulse. The spectrum of the transmitted part of the chirped pulse (3) is collected by an optical fiber and measured by a spectrometer. This spectrum has a cutoff that encodes the arrival time of the short pulse.

### *2.2. Delay measurement technique*

A schematic of the time delay measurement, which is based on nonlinear optical effects and spectral encoding of the delay[31], is shown in Figure 2. Laser pulses from the two sources were focused on the same spot on a dielectric transparent target. Here, we used a cyclic olefin polymer tape (microfluidic ChipShop, Zeonor), 100 μm thick, 24.5 mm wide and 5 m long, which was spooled at a speed of around 0.5 mm/s to provide a fresh undamaged surface for each shot. Pulse 1 (the pump, short pulse) was temporally compressed to 23 fs and had an intensity above $10^{15}$ W/cm$^2$, sufficient to generate a 'plasma mirror' on the target[35]. Pulse 2 (the probe, long pulse) was stretched to approximately 1.1 ps and had an intensity below the ablation threshold (see the Supplementary Information for details on pulse duration setting and characterization). Part of Pulse 2 will be reflected by the plasma mirror if it overlaps temporally with Pulse 1. Since Pulse 2 is chirped, this results in a cutoff in its spectrum, which was recorded by a spectrometer (see Figure S2 in the Supplementary Information). The wavelength of the cutoff depends on the time delay between pulses, whose value multiplied with the speed of light is the optical path length difference (OPLD) between the two laser arms.

### *2.3. Measurement of the delay between pulses from the two HPLS arms*

An initial delay measurement between the two arms was performed at the input of the delay measurement setup (see Figure 1), using two photodiodes with 35 ps rise time (ALPHALAS, UPD-35-UVIR-P) and an oscilloscope with 6 GHz bandwidth (Tektronix, DPO72004C). The initial OPLD between the two arms was 7.2 m, with the long pulses from HPLS Arm B arriving first. A coarse optical delay line was installed on Arm B of the laser system (see Figure 1) to reduce the OPLD to 0.5 m.

The delay measurement setup is illustrated in Figure 3. The pulses were sampled from the center of the two main laser beams using irises, and brought into the same horizontal plane using periscopes. The short pulse (23 fs, 8 mJ) was focused on the transparent target using a 1 m focal length plano-convex lens. The long pulse (1.1 ps, 25 μJ) passed first through an optical delay line with 20 nm resolution (Newport, M-ILS100PP translation stage with an XPS-Q8 controller). Then, a quarter-wave plate in double-pass configuration and a polarizing beamsplitter cube were used to switch the polarization of the long pulse from horizontal

https://doi.org/10.1017/hpl.2024.54 Published online by Cambridge University Press

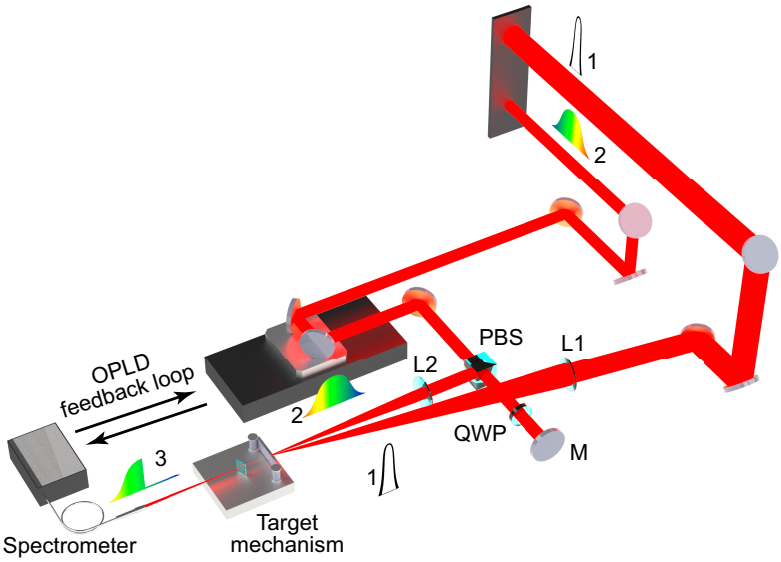


**Figure 3.** Key components of the femtosecond delay measurement setup. 1, pump pulse (8 mJ, $D = 50$ mm); 2, stretched probe pulse (25 μJ, $D = 20$ mm); 3, probe after spectral cut; DL, motorized delay stage; PBS, polarizing beamsplitter cube; QWP, quarter-wave plate, L1, pump focusing lens ($f = 1$ m, $D = 76.2$ mm); L2, probe focusing lens ($f = 0.6$ m, $D = 25.4$ mm).

to vertical. A 0.6 m focal length plano-convex lens focused the long pulse on the target. After the target, the long pulse passed through a polarizer (Thorlabs, PBS25-780-1" polarizing beamsplitter cube) that deflected any components of the short pulse, and then the spectrum of the long pulse was recorded with a fiber-coupled spectrometer (Ocean Optics, D6000).

The delay measurements were performed during a machine beamtime at the ELI-NP facility. The data were recorded in experimental 'runs' during which different measurements were made using consecutive HPLS pulses. For calibration runs, the delay stage was moved in constant increments while the cutoff in the spectrum was measured (see Figures S2–S4 in the Supplementary Information). For free-running measurements, the delay stage was fixed, and the variations of the time delay were observed as variations of the cutoff wavelength. For measurements in which the delay was controlled by a feedback loop, a proportional–integral algorithm was used to calculate delay corrections that were implemented by the delay stage (see the Supplementary Information).

## 3. Results

### *3.1. Spectrum cutoff and plasma mirror properties*

The rapid formation of the plasma mirror is the key phenomenon that enables the high resolution of our delay measurements. For measuring delays, the main concern is a rapid and reproducible generation of the plasma mirror. The generation may be affected by fluctuations of the short-pulse properties, but these properties were stable enough that we did not observe such an impact experimentally.

The stability of the spectra and energies of both pulses was evaluated using the diagnostics integrated in the HPLS, and is illustrated in Figure S5 in the Supplementary Information. Over the range with high spectral intensities (770–820 nm), the relative standard deviation of spectral intensities and the relative differences between runs were around 0.1 or smaller. The ratio of the standard deviation to the average of the pulse energies was 0.02–0.025 for the short pulse and 0.05–0.06 for the long pulse.

We estimated that the plasma mirror had a roughly circular shape with a diameter around 150 μm. This estimate assumes that the plasma mirror had the same shape as the opaque ablated region imprinted on the tape. The darkened region had a roughly constant size during the experiment (see Figure S1 in the Supplementary Information). We estimated the size of the area illuminated by the long pulse by imaging the beam at the tape location (see Figure S1 in the Supplementary Information). The long pulse was approximately 120 μm in size with a 40 μm high-intensity region, and could fit completely inside the mirror area.

During measurements, the alignment of the long pulse inside the plasma mirror area was confirmed by the extinction of the spectral intensity after the cutoff. Without proper alignment, the cutoff was not observed, or a residual intensity was present after the cutoff if part of the probe beam did not overlap with the mirror. The alignment of the two pulses was stable during an experimental run.

In principle, the formation of the mirror could be accelerated by the presence of the long pulse, but this effect was too small to be detectable. Based on the pulse durations, pulse

https://doi.org/10.1017/hpl.2024.54 Published online by Cambridge University Press

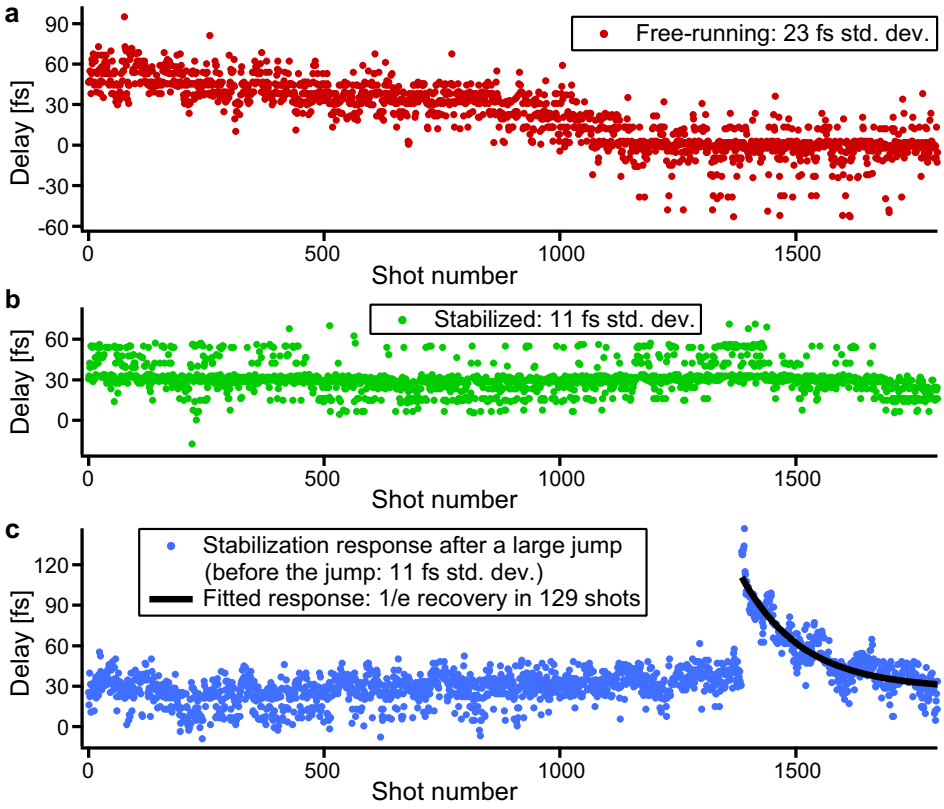


**Figure 4.** Time delay between the 1 PW outputs at 1 Hz repetition rate. (a) Free-running operation. (b) Operation with closed feedback loop. (c) Response of the feedback loop after a large jump in the delay.

energies and beam sizes, the intensity of the long pulse at the mirror is three orders of magnitude lower than that of the short pulse. This small additional intensity should not affect the measured delay, because much larger variations of the energy of the short pulse did not lead to an observable shift of the measured delay (see Figure S6 in the Supplementary Information).

Since the spectrum of the long pulse encodes its time delay, the wavelength interval of the cutoff can be used to estimate the turn-on time of the plasma mirror. This approach characterizes the turn-on time of the mirror's ability to block light, which is one of its essential properties. The transition between 90% and 10% transmission occurred in approximately 100 fs, and Figure S7 in the Supplementary Information shows histograms of the transition time for individual shots. This value represents an upper estimate for the transition time of the transmission, because the transition could be broadened by experimental factors. For example, if the short pulse is not perfectly perpendicular to the target, the plasma mirror would form in a sweeping motion and the duration of the sweep would be added to the transition time. For a maximum plausible misalignment around 10° and a probe spot size of 40 μm, the sweep of the plasma mirror would add around 20 fs to the reflectivity turn-on time.

Although the measured transmission turn-on time is longer than the duration of the short pulse, the precision of the delay measurements is smaller than the turn-on time, because this precision improves proportionally to the resolution with which a spectral intensity level in the cutoff region can be discriminated. In our spectra, this resolution was much better than the range of intensities across the cutoff. We calculated the cutoff as the average of the cutoffs at 40% and 60% of the average spectral intensity between 771.6 and 775.9 nm, a region of the spectrum that had a large intensity and was far from the edge.

### *3.2. Free-running operation*

To quantify the stability of the delay, we define the DS as the standard deviation of all delay measurements from a data set. We recorded the delays while operating the 1 PW dual output at its nominal pulse rate of 1 Hz.

Figure 4(a) shows the evolution of the delay over 30 minutes of continuous operation. A short-term jitter and a long-term drift are apparent in the image, and upon closer inspection we also observed medium-term variations of the delay (see Figure S8(a) in the Supplementary Information). The DS for the data was 23 fs, and the average delay drifted by approximately 50 fs over 30 minutes, corresponding to a drift rate around 100 fs/h. Since we observed drift rates of this magnitude multiple times during the beamtime, we

https://doi.org/10.1017/hpl.2024.54 Published online by Cambridge University Press

estimate that this is a typical drift rate at the 1 PW output of the ELI-NP facility.

### 3.3. Correction of the drift using the feedback loop

Figures 4(b) and 4(c) show two measurements made while the feedback loop was active. Operation with the feedback loop reduced the DS to 11 fs, which is approximately half of the 23 fs standard deviation of the entire free-running data set in Figure 4(a).

During the measurement shown in Figure 4(c), the delay between the two arms exhibited a large jump of about 100 fs. We observed such jumps at varying intervals of the order of 1 hour. The feedback loop corrected this jump with an exponential relaxation time of 129 s (corresponding to 129 pulses). This relatively long relaxation time is due to the insufficiently optimized feedback loop, which is also likely responsible for the slow residual variations of the average delay from Figures 4(b) and 4(c). The slow response of the feedback loop is not a fundamental limitation. We performed virtual stabilization tests of the free-running data (see Figure S10 in the Supplementary Information), which suggest that the delay jumps can be stabilized in approximately 10 s.

During the closed-loop stabilization experiments, we did not identify phenomena that would prevent the stabilization of the time delay over a full day of operation. We did not stabilize the delay over longer periods, because we favored testing multiple target and feedback loop settings during the available beam time.

The stabilization of drifts can be implemented for user experiments by measuring the time delay near the experiment and applying the timing corrections at the front-end after the beams are split. Since the turn-on time of the mirror is longer than the compressed pulse duration, the stabilization could produce two approximately 23 fs compressed pulses that arrive at the sample within approximately 100 fs turn-on time, with a relative delay stable to 11 fs, but do not overlap temporally. Thus, an independent confirmation of the temporal overlap of the two compressed pulses might also be necessary. The overlap could be confirmed through interferometry[26–28] or by monitoring the conversion efficiency of a nonlinear optical process, such as second harmonic generation.

## 4. Discussion

The measurements did not include an additional independent measurement of the delay, from which the precision of the delay measurements can be directly estimated[29,32]. Instead, we estimated a 5 fs upper limit for the precision using a 16-point running standard deviation of the delays. This reached a minimum value of approximately 5 fs over 9 or 10 consecutive measurements (see Figure S8(b) in the Supplementary Information).

Our delay measurements had two main limitations. Firstly, the vertical distribution of time delays in Figure 4 is not uniform, and some delay values occur with very low probability. This behavior was caused by modulations of the wavelength spectrum (see Figures S2 and S3 in the Supplementary Information). Such modulations are difficult to avoid in a laser system where the spectrum is modified by nonlinear effects and reshaped between amplification stages[19]. Secondly, the spectral cutoff was not sharp and corresponded to a turn-on time of approximately 100 fs (see Figure S7, Supplementary Information).

Here, we used the rapid turn-on of the plasma mirror as an empirical phenomenon that enabled precise delay measurements. The ability to measure time delays with a precision of the order of 10 fs was implicitly validated by calibration of the wavelength edge against an externally controlled delay, and by the success of the active stabilization of the delay. However, some properties of the plasma mirror cannot be determined with our setup, for example the delay between the arrival of the pump pulse and reaching a certain reflectivity level. The delay of the mirror should depend on the properties of the short pulse, but we did not observe a correlation between its energy and the delay between pulses (see Figure S6 in the Supplementary Information). Thus, any delay in the mirror formation was practically constant over the narrow range of pulse energies we used, and a constant delay cannot be detected from measurements of delay drift and jitter. Nevertheless, the precision and accuracy of our method may benefit from further studies focused on the dynamics of the plasma mirror, for example by testing a wider range of short-pulse energies, by measuring both the transmission and the reflection of the mirror, or by modeling the formation of the plasma mirror.

## 5. Conclusion

The standard deviation of the short-term delay variations and the DS with the feedback loop are both of the order of 10 fs, which corresponds to a jitter of the OPLD of only 3 μm after 170 m of propagation in each of the arms, a relative variation of $1.8 \times 10^{-8}$. This result validates the design of the ELI-NP facility, which minimizes vibrations and changes in temperature and humidity.

For the delay data shown in Figure 4(b), if both pulses are compressed, 73% of the pulse pairs would overlap by at least half the pulse length. Thus, with delay stabilization and independent confirmation of compressed pulse superposition, many of the double-pulse experiments that require temporal pulse overlap, or delays controlled to 10 fs accuracy, can be run at high data rates because a large fraction of the pulse pairs will have substantial temporal overlap.

https://doi.org/10.1017/hpl.2024.54 Published online by Cambridge University Press

**Acknowledgements**

The authors thank Elena Stroici, Daniel Popa, ThalesLas and the ELI-NP laser operating teams for technical assistance. The ELI-NP team was funded through the IOSIN program, through Nucleu PN-IFIN-HH 23-26 Code PN 23 21, through ELI-NP Phase II, a project co-financed by the Romanian Government and the European Union through the European Regional Development Fund and the Competitiveness Operational Programme (1/07.07.2016, COP, ID 1334), through project PCE 232/2021 PN-III-P4-ID-PCE-2020-2642 and through project ELI-RO/DFG/2023_001 ARNPhot funded by Institute of Atomic Physics Romania. This project has received funding by the European Union's Horizon 2020 Framework Programme grant agreement number 871161 (IMPULSE). C.A.S. acknowledges support from UEFISCDI under PN-IV-2.2-MCD-2023-0045, mobilities program.

**Author contributions**

Conceptualization and supervision: D.U.; experimental setup implementation: A.B.N., S.P., A.M.L., A.D., C.A.S. and D.U.; feedback loop implementation: D.G.M., C.A.S., D.U.; laser operation supervision: D.N., A.T., L.V.; data analysis: A.B.N., S.P., D.G.M., I.D., C.A.S. and D.U.; writing – original draft preparation: A.B.N., S.P., D.G.M., C.A.S. and D.U.; writing – review and editing: D.G.M., I.D., C.A.S. and D.U.; visualization: A.B.N., S.P., D.G.M. and C.A.S.

**Supplementary material**

The supplementary material for this article can be found at https://doi.org/10.1017/hpl.2024.54.

**References**

1. J. W. Yoon, Y. G. Kim, I. Choi, J. H. Sung, H. W. Lee, S. K. Lee, and C. H. Nam, Optica **8**, 630 (2021).
2. A. Di Piazza, C. Müller, K. Z. Hatsagortsyan, and C. H. Keitel, Rev. Mod. Phys. **84**, 1177 (2012).
3. A. Gonoskov, G. Blackburn, M. Marklund, and S. S. Bulanov, Rev. Mod. Phys. **94**, 045001 (2022).
4. P. Zhang, S. S. Bulanov, D. Seipt, A. V. Arefiev, and A. G. R. Thomas, Phys. Plasmas **27**, 050601 (2020).
5. J. M. Cole, K. T. Behm, E. Gerstmayr, T. G. Blackburn, J. C. Wood, C. D. Baird, M. J. Duff, C. Harvey, A. Ilderton, A. S. Joglekar, K. Krushelnick, S. Kuschel, M. Marklund, P. McKenna, C. D. Murphy, K. Poder, C. P. Ridgers, G. M. Samarin, G. Sarri, D. R. Symes, A. G. R. Thomas, J. Warwick, M. Zepf, Z. Najmudin, and S. P. D. Mangles, Phys. Rev. X **8**, 011020 (2018).
6. K. Poder, M. Tamburini, G. Sarri, A. Di Piazza, S. Kuschel, C. D. Baird, K. Behm, S. Bohlen, J. M. Cole, J. Corvan, M. Duff, E. Gerstmayr, C. H. Keitel, K. Krushelnick, S. P. D. Mangles, P. McKenna, C. D. Murphy, Z. Najmudin, C. P. Ridgers, G. M. Samarin, D. R. Symes, A. G. R. Thomas, J. Warwick, and M. Zepf, Phys. Rev. X **8**, 031004 (2018).
7. C. A. Lindstrom, Phys. Rev. Accel. Beams **24**, 014801 (2021).
8. S. Steinke, J. van Tilborg, C. Benedetti, C. G. R. Geddes, C. B. Schroeder, J. Daniels, K. K. Swanson, A. J. Gonsalves, K. Nakamura, N. H. Matlis, B. H. Shaw, E. Esarey, and W. P. Leemans, Nature **530**, 190 (2016).
9. J. Magnusson, A. Gonoskov, M. Marklund, T. Z. Esirkepov, J. K. Koga, K. Kondo, M. Kando, S. V. Bulanov, G. Korn, C. G. R. Geddes, C. B. Schroeder, E. Esarey, and S. S. Bulanov, Phys. Rev. A **100**, 063404 (2019).
10. J. Ferri, E. Siminos, and T. Fülöp, Commun. Phys. **2**, 40 (2019).
11. B. King, A. Di Piazza, and C. H. Keitel, Nat. Photonics **4**, 92 (2010).
12. B. Kettle, D. Hollatz, E. Gerstmayr, G. M. Samarin, A. Alejo, S. Astbury, C. Baird, S. Bohlen, M. Campbell, C. Colgan, D. Dannheim, C. Gregory, H. Harsh, P. Hatfield, J. Hinojosa, Y. Katzir, J. Morton, C. D. Murphy, A. Nurnberg, J. Osterhoff, G. Pérez-Callejo, K. Poder, P. P. Rajeev, C. Roedel, F. Roeder, F. C. Salgado, G. Sarri, A. Seidel, S. Spannagel, C. Spindloe, S. Steinke, M. J. V. Streeter, A. G. R. Thomas, C. Underwood, R. Watt, M. Zepf, S. J. Rose, and S. P. D. Mangles, New J. Phys. **23**, 115006 (2021).
13. C. J. Hooker, J. L. Collier, O. Chekhlov, R. Clarke, E. Divall, K. Ertel, B. Fell, P. Foster, S. Hancock, A. Langley, D. Neely, J. Smith, and B. Wyborn, J. Phys. IV France **133**, 673 (2006).
14. J. H. Sung, H. W. Lee, J. Y. Yoo, J. W. Yoon, C. W. Lee, J. M. Yang, Y. J. Son, Y. H. Jang, S. K. Lee, and C. H. Nam, Opt. Lett. **42**, 2058 (2017).
15. T. J. Yu, S. K. Lee, J. H. Sung, J. W. Yoon, T. M. Jeong, and J. Lee, Opt. Express **20**, 10807 (2012).
16. M. Cerchez, R. Prasad, B. Aurand, A. L. Giesecke, S. Spickermann, S. Brauckmann, E. Aktan, M. Swantusch, M. Toncian, T. Toncian, and O. Willi, High Power Laser Sci. Eng. **7**, e37 (2019).
17. L. Volpe, R. Fedosejevs, G. Gatti, J. A. Pérez-Hernández, C. Méndez, J. Apiñaniz, X. Vaisseau, C. Salgado, M. Huault, S. Malko, G. Zeraouli, V. Spina, A. Longman, D. De Luis, K. Li, O. Varela, E. García, I. Hernandez, J. D. Pisonero, J. G. Ajates, J. M. Alvarez, C. García, M. Rico, D. Arana, J. Hernández-Toro, and L. Roso, High Power Laser Sci. Eng. **7**, e25 (2019).
18. E. Kroupp, S. Tata, Y. Wan, D. Levy, S. Smartsev, E. Y. Levine, O. Seemann, M. Adelberg, R. Piliposian, T. Queller, E. Segre, K. T. Phuoc, M. Kozlova, and V. Malka, Matter Radiat. Extrem **7**, 044401 (2022).
19. F. Lureau, G. Matras, O. Chalus, C. Derycke, T. Morbieu, C. Radier, O. Casagrande, S. Laux, S. Ricaud, G. Rey, A. Pellegrina, C. Richard, L. Boudjemaa, C. Simon-Boisson, A. Baleanu, R. Banici, A. Gradinariu, C. Caldararu, B. De Boisdeffre, P. Ghenuche, A. Naziru, G. Kolliopoulos, L. Neagu, R. Dabu, I. Dancus, and D. Ursescu, High Power Laser Sci. Eng. **8**, e43 (2020).
20. C. Radier, O. Chalus, M. Charbonneau, S. Thambirajah, G. Deschamps, S. David, J. Barbe, E. Etter, G. Matras, S. Ricaud, V. Leroux, C. Richards, F. Lureau, A. Baleanu, R. Banici, A. Gradinariu, C. Caldararu, C. Capiteanu, A. Naziru, B. Diaconescu, V. Iancu, R. Dabu, D. Ursescu, I. Dancus, C. A. Ur, K. A. Tanaka, and N. V. Zamfir, High Power Laser. Sci. Eng. **10**, e21 (2022).
21. J. Nees, A. Maksimchuk, G. Kalinchenko, B. X. Hou, Y. Ma, P. Campbell, A. McKelvey, L. Willingale, I. Jovanovic, C. Kuranz, A. Thomas, and K. Krushelnick, in *2020 Conference on Lasers and Electro-Optics (CLEO)* (2020), paper JW2B.9.
22. C. N. Danson, C. Haefner, J. Bromage, T. Butcher, J. C. F. Chanteloup, E. A. Chowdhury, A. Galvanauskas, L. A. Gizzi, J. Hein, D. I. Hillier, N. W. Hopps, Y. Kato, E. A. Khazanov, R. Kodama, G. Korn, R. X. Li, Y. T. Li, J. Limpert, J. G. Ma, C. H. Nam, D. Neely, D. Papadopoulos, R. R. Penman, L. J. Qian, J. J. Rocca, A. A. Shaykin, C. W. Siders, C. Spindloe, S.

Szatmári, R. Trines, J. Q. Zhu, P. Zhu, and J. D. Zuegel, High Power Laser Sci. Eng. **7**, e54 (2019).
23. P. T. Callahan, K. Safak, P. Battle, T. D. Roberts, and F. X. Kärtner, Opt. Express **22**, 9749 (2014).
24. N. Prakash, S. W. Huang, and B. W. Li, Optica **9**, 717 (2022).
25. R. A. Yang, M. H. Zhao, X. G. Jin, Q. Li, Z. Y. Chen, A. M. Wang, and Z. G. Zhang, Optica **9**, 874 (2022).
26. D. J. Corvan, T. Dzelzainis, C. Hyland, G. Nersisyan, M. Yeung, M. Zepf, and G. Sarri, Opt. Express **24**, 3127 (2016).
27. D. Kim, C. I. Hojbota, M. Mirzaie, S. K. Lee, K. Y. Kim, J. H. Sung, and C. H. Nam, Rev. Sci. Instrum. **93**, 113001 (2022).
28. D. Meshulach, D. Yelin, and Y. Silberberg, J. Opt. Soc. Am. B **14**, 2095 (1997).
29. R. Shalloo, C. Arran, G. Cheung, L. Corner, J. Holloway, R. Walczak, S. Hooker, N. Booth, O. Chekhlov, and C. Gregory, "Measurement of femtosecond-scale drift and jitter of the delay between the North and South Beams of Gemini," Central Laser Facility Annual Report #36 (Central Laser Facility, UK, 2015).
30. Y. Wan, O. Seemann, S. Tata, I. A. Andriyash, S. Smartsev, E. Kroupp, and V. Malka, Nat. Phys. **18**, 1186 (2022).
31. R. G. Ungureanu, G. V. Cojocaru, R. A. Banici, and D. Ursescu, Opt. Express **22**, 15918 (2014).
32. M. Harmand, R. Coffee, M. R. Bionta, M. Chollet, D. French, D. Zhu, D. M. Fritz, H. T. Lemke, N. Medvedev, B. Ziaja, S. Toleikis, and M. Cammarata, Nat. Photonics **7**, 215 (2013).
33. B. Brizard, A. Leblanc, S. Petit, J. C. Delagnes, É. Cormier, H. Ibrahim, F. Légaré, and P. Lassonde, Opt. Express **28**, 35807 (2020).
34. R. H. Sawicki, Proc. SPIE **5341**, 43 (2004).
35. C. Thaury, F. Quéré, J. P. Geindre, A. Levy, T. Ceccotti, P. Monot, M. Bougeard, F. Reau, P. D'Oliveira, P. Audebert, R. Marjoribanks, and P. H. Martin, Nat. Phys. **3**, 424 (2007).

https://doi.org/10.1017/hpl.2024.54 Published online by Cambridge University Press